Probing the protein corona of gold/silica nanoparticles by Taylor dispersion analysis-ICP-MS

Arthur Degasperi, Lucie Labied, Carole Farre, Emmanuel Moreau, Matteo Martini, Carole Chaix, Agnès Hagège

▶ **To cite this version:**

Arthur Degasperi, Lucie Labied, Carole Farre, Emmanuel Moreau, Matteo Martini, et al.. Probing the protein corona of gold/silica nanoparticles by Taylor dispersion analysis-ICP-MS. Talanta, 2022, 243, pp.123386. 10.1016/j.talanta.2022.123386 . hal-03663936

HAL Id: hal-03663936
https://hal.science/hal-03663936v1

Submitted on 10 May 2022

HAL is a multi-disciplinary open access archive for the deposit and dissemination of scientific research documents, whether they are published or not. The documents may come from teaching and research institutions in France or abroad, or from public or private research centers.

L'archive ouverte pluridisciplinaire **HAL**, est destinée au dépôt et à la diffusion de documents scientifiques de niveau recherche, publiés ou non, émanant des établissements d'enseignement et de recherche français ou étrangers, des laboratoires publics ou privés.

Probing the protein corona of gold/silica nanoparticles by Taylor Dispersion Analysis-ICP-MS

Arthur Degasperi[1], Lucie Labied[1], Carole Farre[1], Emmanuel Moreau[2], Matteo Martini[3], Carole Chaix[1], Agnès Hagège[1*]

[1]Université de Lyon, CNRS, Université Claude Bernard Lyon 1, Institut des Sciences Analytiques, UMR 5280, 69100 Villeurbanne, France.

[2] Université Clermont Auvergne, Imagerie Moléculaire et Stratégies Théranostiques, Inserm, U 1240, Centre Jean Perrin BP 184, F-63011, Clermont-Ferrand, France.

[3]Institut Lumière Matière, Université Claude Bernard Lyon 1, CNRS UMR 5306, 69622 Villeurbanne, France.

*Corresponding author : Agnès Hagège, Institut des Sciences Analytiques, UMR 5280, 5 rue de la Doua, 69100 Villeurbanne, France, e-mail : agnes.hagege@isa-lyon.fr, phone +(33) 437.423.550

ABSTRACT: Despite the tremendous interest for nanoparticles (NPs) in the biomedical field, their transfer to the clinics is still hampered, in particular due to the lack of knowledge of their behaviour in a biological environment. Indeed, the protein corona formed as soon as NPs enter the bloodstream can drastically affect their properties. The use of Taylor dispersion analysis-ICP-MS as an efficient technique dedicated to metal-containing NPs was proposed to examine these NP−protein interactions and determine protein corona thicknesses in biological fluids. This method was applied on core-shell gold/silica NPs in the presence of proteins at high concentrations and serum. Protein corona around 4 nm were measured. Moreover, the versatility of the method allowed assessing the reversible/irreversible character of the interactions.

Keywords: Taylor dispersion analysis, Inductively coupled plasma mass spectrometry, Metal-containing nanoparticles, Protein corona, Reversible interactions, Albumin

1. Introduction

Metal-containing nanoparticles (NPs) are increasingly investigated in the biomedical field. This burgeoning technology enables to explore various alternative strategies, in the field of both diagnosis and therapy [1,2]. However, the development of effective therapeutic strategies is based on the understanding of the *in vivo* behavior of NPs. As they enter the bloodstream, NPs may be rapidly surrounded by a wide variety of biomolecules, in particular proteins, which adsorb on their surface and may completely cover them. This protein corona modifies the physicochemical characteristics of the pristine NPs and constitutes the first contact of the nanomaterial with the cells. It is therefore susceptible not only to modify the absorption pathways of NPs but also to generate an additional level of complexity [3-5]. Milani *et al.* demonstrated that proteins involved in this corona exhibit very distinct kinetics of dissociation. The so-called "hard corona" is assumed to be irreversible while the "soft corona" shows fast off-rates (in the range of a minute) [6]. Due to the difficulty to preserve the soft corona, its potential occurrence has been often overlooked. Apart from a few studies reporting that soft corona proteins may contribute to the stealth properties of nanoparticles [7] or affect the attachment efficiency of NPs to biological membranes [8], the role of this soft corona remains elusive. Much research has been performed to identify the proteins forming the corona by mass spectrometry [9-11]. However, the usual procedures imply the previous separation of the NPs from the biological fluids, leading then to the loss of proteins with fast dissociation kinetics.

The number of proteins involved in the hard corona of gold NPs was determined by laser induced breakdown spectroscopy, using the plasmonic features of gold NPs [12]. An alternative approach used capillary-ICP-MS hyphenation to separate free NPs from Au-NP-protein conjugates. It demonstrated the replacement of initially adsorbed transferrin on the particle surface by albumin with time [13]. Moreover, the determination of the number of albumin involved in the conjugate was realized by quantifying Au, referring to the NP, and S referring to the protein [14].

Characterization of protein adsorption can also be performed through NP size measurements. When NPs are suspended in biological media, protein adsorption on their surface results in an increased size of the NPs, due to protein adsorption. Therefore, corona thickness can be deduced from NP sizes measured in media either free or containing proteins. However, measuring a protein corona of a few nanometers is intricate. Only few techniques do not require sample treatment before analysis, so as not to disturb the equilibrium of the protein corona and its properties. The most popular technique for NPs size measurements is dynamic light scattering (DLS). However, the scattering intensity of NPs in DLS is often much smaller as compared to that of serum [15]. For that reason, DLS measurements are often conducted in diluted media. Due to the low contrast generated by proteins, transmission electron microscopy (TEM) requires the addition of a contrast agent (generally uranyl acetate), which precludes its use *in situ* [16]. Therefore, alternatives methods were developed. In a recent work, Galdino *et al.* studied the process of protein corona formation on silica NPs by core-loss energy-filtered TEM and cryo-TEM. They successfully measured corona thicknesses of 4 - 9 nm. Small-angle X-ray scattering (SAXS) was also used to determine binding parameters in the presence of both BSA and serum [17]. Although very sensitive, SAXS revealed insufficiently accurate measurements of the protein corona thickness. Nevertheless, it seems to be the only technique reported to distinguish between protein corona and aggregation. In the case of fluorescent NPs, fluorescence correlation spectroscopy (FCS) was used for determination of the protein corona thickness in media containing proteins with concentrations close to the ones encountered in serum. Corona thicknesses of a few nanometers were successfully measured on a wide variety of NPs [18-20].

We recently showed that Taylor dispersion analysis hyphenation to inductively coupled plasma mass spectrometry (TDA-ICP-MS) is particularly adapted for metal-containing NP size measurements [21,22]. Furthermore, thanks to the selectivity of the technique to metals, TDA-ICP-MS allows size measurements to be performed in complex matrices, rich in proteins, whereas these measurements are often not possible by DLS. Herein, we devised a methodology based on the monitoring of the metal signal, which enables not only to measure the protein corona thickness onto NPs, but also to gain

information about the reversibility of this adsorption. As a proof-of-principle, the method was applied using 60 nm core-shell gold/silica nanoparticles (Au@SiO_x NPs) suspended in protein-rich model solutions and serum.

2. Materials and methods

2.1. Chemicals and solutions

Triton X-100, n-hexanol, cyclohexane, $HAuCl_4 \cdot 3H_2O$, sodium 2-mercaptoethanesulfonate (MES), $NaBH_4$, tetraethoxysilane (TEOS), and (3-aminopropyl)triethoxysilane (APTES), purchased from Aldrich, NH_4OH, purchased from Chimie Plus, and 3-(Triethoxysilyl)propylsuccinic anhydride (Si-20), purchased from ABCR were used for Au@SiO_x nanoparticles synthesis.

Disodium hydrogen phosphate dihydrate, sodium dihydrogen phosphate dihydrate and sodium chloride from Sigma-Aldrich were all of analytical grade. Nitric acid 1 $mmol.L^{-1}$ was obtained by dilution of HNO_3 Suprapur® (Merck). Bovine serum albumin (BSA) and fetuin from fetal calf serum (FET) were purchased from Sigma-Aldrich. Solutions of proteins were freshly prepared. Control of protein aggregation was performed by TDA-UV.

Serum from human male AB plasma (H4522) was also purchased from Sigma-Aldrich.

All aqueous solutions used for both synthesis and analytical experiments were prepared with ultrapure water (18.2 MΩ cm resistivity, Milli-Q station, Merck Millipore).

Silica capillaries (Photonlines, length 70 cm, 75 µm i.d., 375 µm o.d.) were coated with hydroxylpropylcellulose (HPC) prior to use by flushing a HPC (0.1% w/w in water) under 4 bar for 15 min, then heating them at 140°C for 30 min under a N_2 stream (1 bar).

2.2. Synthesis of the Au@SiO_x NPs

Au@SiO_x NPs were prepared according to a method developed by Martini *et al.* [23]. Quaternary W/O microemulsion was prepared by mixing 11.5 mL of Triton X-100 (surfactant), 11.5 mL of n-hexanol (co-

surfactant), 48 mL of cyclohexane (oil). The water phase consists of mixture of 3 mL of 16.7 mmol.L^{-1} $HAuCl_4 \cdot 3H_2O$, 3 ml of 32.8 mmol.L^{-1} MES and 1 mL of 412 mmol.L^{-1} $NaBH_4$ in order to synthesize the gold nanoparticle. After 5 min, 0.050 mL of APTES was added to the microemulsion solution, followed by 0.2 mL of TEOS. After 30 min, the silica polymerization reaction was completed by adding 0.2 mL of NH_4OH and then stirring for 24 h. In order to achieve the colloidal stability, a carboxylated protective shell was created by adding 0.02 mL of Si-20. The microemulsion was broken by the addition of ethanol to the microemulsion and followed by vortexing and centrifuging several times. Unreacted precursors were removed by ultrafiltration using 100 kDa polyethersulfone membranes. Particles were dispersed in aqueous solution (2 mg.mL^{-1}) and stored at 4°C. Characterization of NPs is provided as Supplementary material (section 1).

2.3. Taylor dispersion analysis – ICP/MS analysis

A 7100 capillary electrophoresis system (Agilent) was used for TDA analyses.

Detection of gold was enabled by hyphenation with a Nexion 300X ICP-MS (Perkin Elmer). For that purpose, a T-connector was used as sheath-flow interface. The TDA capillary went through a T-connector toward the tip of the nebulizer and the sheath liquid (HNO_3 1 mmol.L^{-1}) was introduced by self-aspiration to the third inlet of the interface. This interface was previously shown not to introduce any external dispersion that could enlarge peaks [21].

Au signal was monitored at m/z 197, with a dwell time of 500 ms. Operating conditions used for the ICP-MS were: nebulizer gas flow rate, 1.09 L/min; plasma gas flow rate, 18 L/min; auxiliary gas flow rate, 1.2 L/min; radiofrequency power, 1600 W for the plasma. All other parameters were tuned to maximize the Au signal.

3D-CE Chemstation software version B.04.03 (Agilent) was used to control the CE system and Syngistix software version 2.3 was used to both control the ICP-MS and acquire the ^{197}Au signal.

Using sodium phosphate mobilization solutions, capillaries were conditioned 10 min at 1 bar. For protein mobilization media, capillaries were conditioned 5 min at 1 bar with the protein solution, then 10 min at 50 mbar.

One $g.L^{-1}$ $Au@SiO_x$ NP suspensions were prepared by addition of an equivalent volume of the incubation medium (sodium phosphate buffer 10 mM, protein solutions, and serum). The $Au@SiO_x$ NP suspensions were kept at room temperature without stirring and aliquots were collected at different times for size measurements.

NPs were injected hydrodynamically under 40 mbar for 3 s in a capillary filled with the desired medium and a mobilization pressure of 50 mbar was applied.

Measurements of hydrodynamic radii in the incubation medium were performed in capillaries filled with the same medium. Assessment of the reversible character of the protein interactions were performed in capillaries filled with 10 mM phosphate buffer, pH 7.4.

2.4. Calculation of the nanoparticle hydrodynamic radius

The detected peak can be fitted by a sum of Gaussian distributions, according to the following equation:

$$S(t) = \sum_{i=1}^{n} \frac{A_i}{\sigma_i \sqrt{2\pi}} \exp\left(-\frac{(t-t_0)^2}{2\sigma_i^2}\right) \quad (1)$$

where i is the number of species, t is the experimental time, t_0, the residence time, σ_i the mean temporal variance of the Gaussian distribution associated to the species i and A_i, a constant depending on the concentration of the species i.

Under experimental conditions described by Chamieh *et al.* [24], the molecular diffusion coefficient D can be obtained using the Stokes–Einstein equation:

$$D = \frac{R_c^2 t_0}{24\sigma^2} = \frac{k_B T}{6\pi\eta R_h} \quad (2)$$

where R_c is the capillary radius, k_B is the Boltzmann constant, T is the temperature, η is the viscosity, and R_h is the hydrodynamic radius of the solute.

The diffusion coefficient, and therefore the hydrodynamic radius of a solute, are then based on the Gaussian fits of the peaks obtained in TDA-ICP-MS realized using the Origin software (version 8.5).

As a tailing deformation induced by retention may occur at the end of the peak, only the first half of the peak can be assimilated to a sum of Gaussians. In theory, a peak half contains all the necessary and sufficient information. However, the noise at the top of the peak can bias the determination of the residence time. Therefore, the time interval over which the adjustment must be made was carefully determined in order to limit both noise and retention effects. Preliminary experiments have shown that 15 to 30% of the second half of the peak must be taken into account.

2.5. *DLS measurements*

Colloidal solutions of $Au@SiO_x$ NPs at 2 $mg.mL^{-1}$ in pure water were used. Measurements were performed using a Zetasizer Nano-S (633 nm He-Ne laser) from Malvern Instruments (USA). Measurements were averaged over 10 individual measurements, performed at 25°C. The validity of the data was determined by examination of both the autocorrelation curves and the quality report.

3. Results and discussion

3.1. Hydrodynamic size of the nanoparticle

Hydrodynamic size measurement of the $Au@SiO_x$ NPs suspended in aqueous solution was performed using both TDA-ICP-MS and DLS (Figure 1).

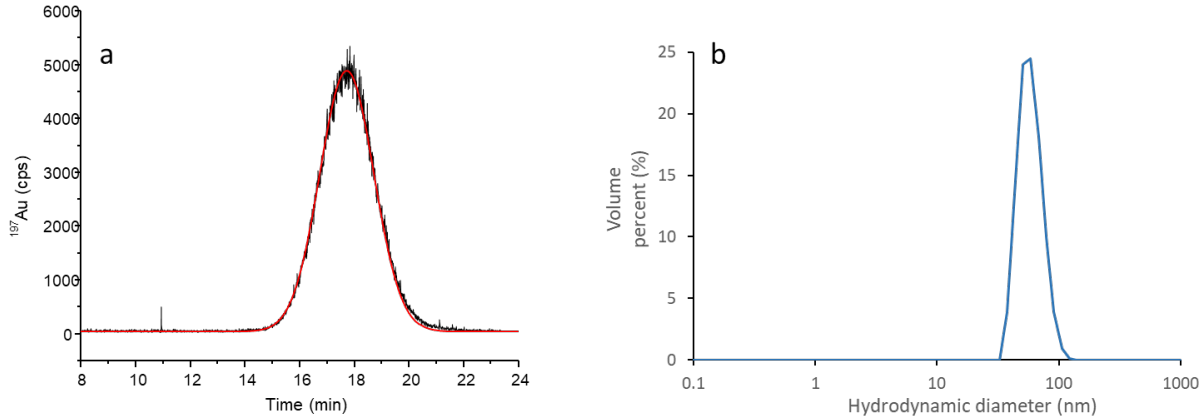

Fig. 1: Comparison of size measurements for Au@SiO_x NPs at 2 mg.mL^{-1} in water a) Representative Taylorgram of Au@SiO_x NPs (black line), with the corresponding Gaussian fitting (red line). Experimental conditions: injection 40 mbar 3 s; HPC capillary 50 µm i.d. x 70 cm length; buffer sodium phosphate 10 mmol.L^{-1}, pH 7.4; mobilization pressure 50 mbar; ICP-MS detection m/z = 197. b) DLS of Au@SiO_x NPs in water.

The hydrodynamic radius obtained with TDA-ICP-MS in 10 mmol.L^{-1} sodium phosphate buffer was found to be (30 ± 1) nm, over 12 repetitions (Fig. 1a). This result is in close agreement with the value obtained by DLS: (30 ± 2) nm (Fig. 1b). The goodness of the fit strongly supports the assumption of the main monodisperse character of the NP, as confirmed by TEM and DLS (see Supplementary material, section 1).

3.2. Measuring the protein corona thickness

TDA-ICP-MS was already demonstrated to successfully measure hydrodynamic radii of NPs in various complex media [22]. The selectivity of the ICP-MS detection, in our case ^{197}Au, allows the only detection of Au compounds and eliminates interference caused by other compounds such as free proteins present in the solution. Thanks to this features, this coupling allows to consider the measurement of the size of NPs in media with high protein contents. For that purpose, two model proteins have been chosen: BSA, which is one of the most studied protein and FET. Moreover, both proteins are important components of many cell culture media (i.e. media containing fetal calf serum). The isoelectric point of FET (pI=5.4) is higher than the one of BSA (pI = 4.7). Both proteins have close molecular weight.

However, in serum, FET concentration (0.4 - 0.9 mg.mL^{-1}) is rather low compared to that of albumin (35 - 55 mg.mL^{-1}), although it is one of the 15 most abundant proteins in serum.

The influence of the concentration of both BSA and FET was investigated. For that purpose, colloidal solutions of Au@SiO$_x$ NPs were incubated at room temperature for at least 24 h with increasing concentrations of both FET and BSA (0 to 30 and 50 mg.mL^{-1}, respectively) in sodium phosphate 10 mmol.L^{-1}, pH 7.4. Prior to incubation, the protein solutions were checked by TDA, using UV detection, in order to ensure the non-aggregation of proteins (see Supplementary material, section 2)

Aliquots were frequently collected (25 µL) for at least 6 h and analysed in a capillary, filled with the same medium than the incubation medium, to ensure the equilibrium between the NPs and the proteins.

Results are presented in Figures 2 and 3 for BSA and FET, respectively.

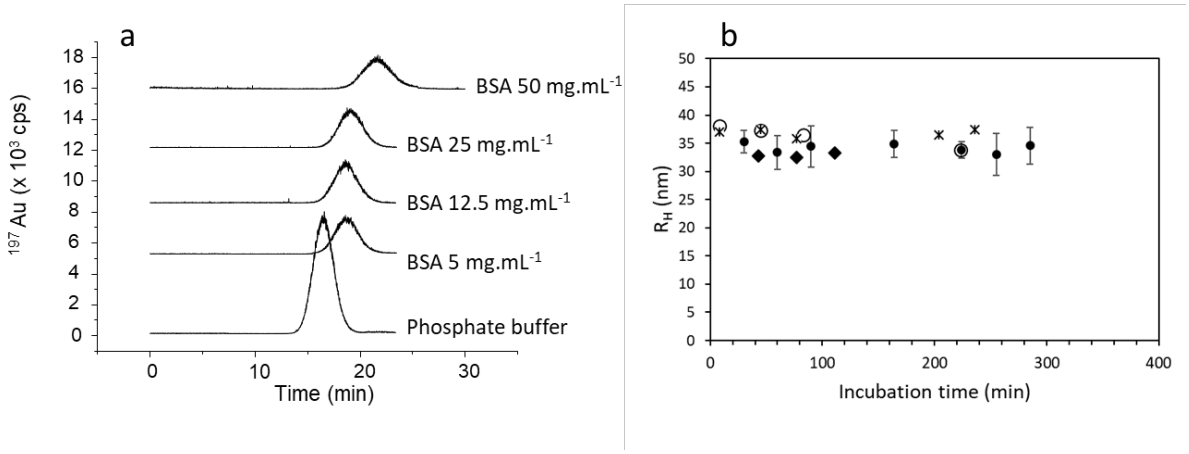

Fig. 2: Influence of BSA concentration on the hydrodynamic radii of Au@SiOx NPs a) Taylorgrams of Au@SiO$_x$ NPs incubated in various BSA solutions. Experimental conditions: Au@SiO$_x$ NPs, either 2 mg.mL^{-1} suspensions in pure water or 1 mg.mL^{-1} suspensions in BSA solutions; injection 40 mbar 3 s; HPC capillary 75 µm i.d. x 70 cm total length; analysis medium: phosphate buffer or BSA solutions; mobilization pressure 50 mbar; ICP-MS detection m/z = 197. Taylorgrams were shifted in intensity for sake of clarity b) Mean hydrodynamic radius of the Au@SiO$_x$ NP as a function of incubation time in BSA solutions: (◆) 5 mg.mL^{-1}, (✳) 12.5 mg.mL^{-1}, (○) 25 mg.mL^{-1}, (●) 50mg.mL^{-1}

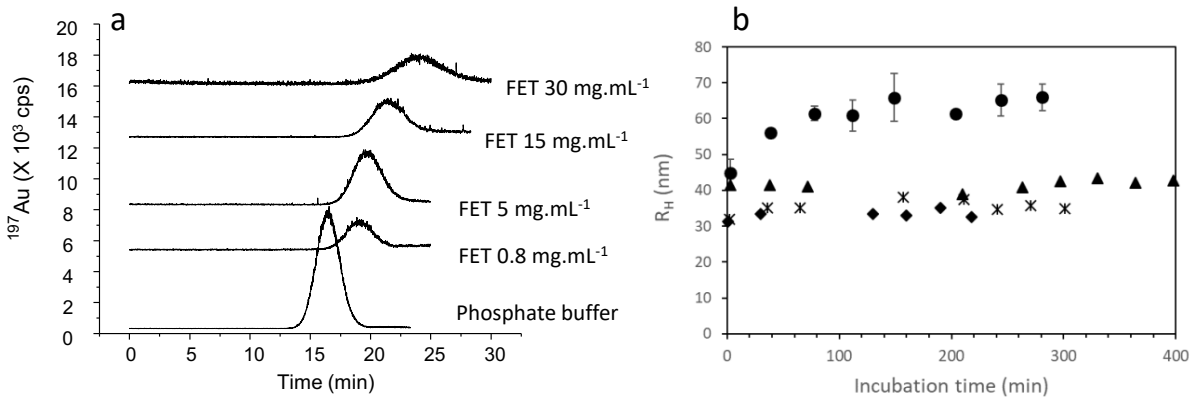

Fig. 3: Influence of FET concentration on the hydrodynamic radii of Au@SiOx NPs a) Taylorgrams of Au@SiO_x NPs incubated in various FET solutions. Experimental conditions: Au@SiO_x NPs, either 2 mg.mL^{-1} suspensions in pure water or 1 mg.mL^{-1} suspensions in FET solutions; injection 40 mbar 3 s; HPC capillary 75 µm i.d. x 70 cm total length; analysis medium: phosphate buffer or FET solutions; mobilization pressure 50 mbar; ICP-MS detection m/z = 197. Taylorgrams were shifted in intensity for sake of clarity b) Hydrodynamic radius of the Au@SiOx NP as a function of incubation time in FET solutions: (◆) 0.8 mg.mL^{-1}, (∗) 5 mg.mL^{-1}, (▲) 15 mg.mL^{-1}, (●) 30mg.mL^{-1}

For each condition, Taylorgrams exhibit a peak, which can be fitted using a single Gaussian. Moreover, the peak areas were found to be constant over the timescale of the experiments, for all the protein concentrations, indicating that the colloidal stability of the NPs is maintained in such media.

The observed variations in average peak residence times as a function of protein concentration are due to the different viscosities of the studied media. As for DLS, the diffusion coefficient, and hence the hydrodynamic radius calculation, depends on viscosity. For that purpose, viscosities were measured in the different media (see Supplementary material, section 3) and used to determine hydrodynamic radii.

Whatever the protein concentration, a rapid increase of the hydrodynamic radius (in less than 20 min) was observed for both proteins. This increase was attributed to the formation of a protein corona around the particle. Values are presented in Table 1. The significance of differences between the data

were determined based on P values < 0.001 by using t-tests (as described in Supplementary Material, section 4)

Table 1.

Mean hydrodynamic radii for $Au@SiO_x$ NPs as a function of the incubation medium

BSA		FET	
[BSA] $mg.mL^{-1}$	Hydrodynamic radius (nm)	[FET] ($mg.mL^{-1}$)	Hydrodynamic radius (nm)
0 (phosphate buffer)	30.0 ± 0.7	0 (phosphate buffer)	30.0 ± 0.7
5	32.8 ± 0.4	0.8	31 ± 1
12.5	36.8 ± 0.7	5	33 ± 1
25	35 ± 2	15	35 ± 1
50	34.2 ± 0.8	30*	62 ± 7

*Hydrodynamic radius was calculated by averaging values at the plateau (time $\geq$ 80 min)

Consequently, protein corona thicknesses can be obtained from the difference ΔR_H, between the hydrodynamic radius obtained in a protein medium (either BSA or FET) and the one obtained in phosphate buffer, recapitulated in Table 1. For both proteins, an increase in hydrodynamic radius was observed.

The isoelectric point of the $Au@SiO_x$ NPs surface, obtained by measuring the zeta potential ζ as a function of pH (see Supplementary material, section 1), was about 4.3, confirming the main presence of carboxylate functions on surface. This value is higher than that conventionally obtained for silica NPs (pI = 3.5) [25]. This difference may be due to the additional presence of both carboxylated groups and ammonium ions originating from APTES on the NP surface [26].

Owing to the pI of both proteins, the question of a heterogeneous spatial distribution of charges should be evoked to explain the protein adsorption onto the NPs, as both proteins and $AuSiO_x$ NPs are negatively charged at pH 7.4.

In the case of BSA, the values obtained for the corona thickness ($\Delta R_H \sim 3 – 7$ nm) seem to be in agreement with the values reported in the literature. The formation of a BSA corona on silica NPs was

studied by other groups and seems to be size-dependent. A corona thickness of 7 nm and 4 nm was reported by Galdino *et al.* for 40 nm and 80 nm – silica NPs respectively [17]. Monopoli *et al.* observed a corona thickness of 4 nm for 200 nm silica NPs [27]. Smaller particles are thought to be more prone to aggregate in the presence of BSA. Orts-Gil *et al.* observed an hydrodynamic radius of ca. 100 nm for 15 nm-silica NPs in BSA solutions, resulting from the formation of NPs-BSA clusters [28] and a small aggregation was also reported by Monopoli *et al.* for 50 nm – silica NPs [27].

A corona thickness of about 3-4 nm for the corona in the presence serum albumin was also observed for other NPs, such as 5 nm-FePt NPs [20], 5 nm-quantum dots [19] and even larger nanoparticles, i.e. polystyrene nanoparticles between 20 and 100 nm [29].

Given the hydrodynamic radius of BSA (4.3 $\pm$ 0.3 nm, see Supplementary material, section 2), this 4 nm-corona may reflect the formation of a BSA monolayer, also indicating the absence of multilayer adsorption. . However, the accuracy of TDA-ICP-MS does not allow us a more thorough interpretation of the recorded ΔR_H until now.

On the contrary, FET adsorption seems to be concentration-dependent. For a FET concentration close to the one of serum (0.8 $mg.mL^{-1}$), no significant adsorption was observed. Increasing concentration in the 5 - 15 $mg.mL^{-1}$ range yielded a corona thickness of ~3 - 5 nm, supporting the assumption of a monolayer adsorption. Indeed, the hydrodynamic radius of FET, measured by TDA – UV (see Supplementary material, section 2) was found to be (4.6 $\pm$ 0.4) nm.

For the highest concentration, similar to the one of BSA in serum, an unexpected increase in R_H was observed. As can been seen in Figure 3b, a gradual increase of the hydrodynamic radius seems to occur upon time, until a plateau is reached for values approximately twice those of the $Au@SiO_x$ NP radius after 80 min incubation.

In the literature, this behaviour was also encountered for 40 nm-silica particles in fetal calf serum, for which a progressive increase in hydrodynamic radius until a value of 37-46 nm was observed by DLS. Based on microscopy data, this was attributed by Galdino *et al.* to the formation of small aggregates

[17]. As TDA experiments showed that FET aggregation did not occur in phosphate buffer using such a concentration (see Supplementary material, section 2), NPs aggregation mediated by proteins might be considered, even if the formation of protein multilayers cannot be excluded in the absence of additional proofs. However, it is worth noting that we did not observe protein aggregates by TDA-UV, in the 30 and 60 mg.mL^{-1} FET solutions (see Supplementary material, section 2).

The method was then applied to the measurement of Au@SiO_x NPs protein corona formed in human serum. Results are presented in Figure 4.

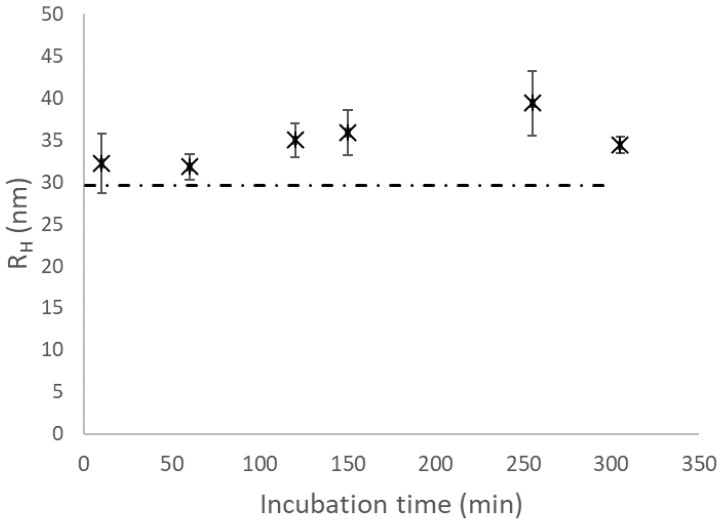

Fig. 4: Hydrodynamic radii of Au@SiO_x NPs as a function of time in different media. Experimental conditions: Au@SiOx NPs, suspended in serum diluted twice (✳) ; injection 40 mbar 3 s; HPC capillary 75 µm i.d. x 70 cm total length; analysis medium: twice diluted serum; mobilization pressure 50 mbar; ICP-MS detection m/z = 197.

In the presence of serum, the hydrodynamic radius of the Au@SiO_x NPs also increases. Although the standard deviation is more important, as for BSA 50 mg.mL^{-1} and FET 30 mg.mL^{-1}, the values obtained for the longest incubation times ((35 $\pm$ 2) nm, (36 $\pm$ 3) nm, and (39 $\pm$ 4) nm, for 120, 150, and 255 min incubation respectively) are significantly higher than the hydrodynamic radius of the NPs in the absence of proteins. As a consequence, the existence of a protein corona of ca. 5 nm-thickness can be postulated.

3.3. Assessing the high binding affinity protein corona

It is now commonly accepted that the protein corona consists in proteins with high binding affinities and therefore low exchange rate, known as «hard corona», but also in a highly dynamic «soft corona», consisting of further adsorbed proteins with low binding affinities and high exchange rates. In order to evaluate the affinity of the proteins forming the corona, Au@SiO_x NPs were incubated in different media (phosphate buffer, protein solutions, diluted serum) for 2 h and were then analysed in a capillary filled with either the incubation medium or the phosphate buffer pH 7.4. Additionally, experiments were also performed in the phosphate buffer after incubation of Au@SiO_x NPs in a BSA solution 50 $mg.mL^{-1}$ for 4 h. Results are presented in Figure 5.

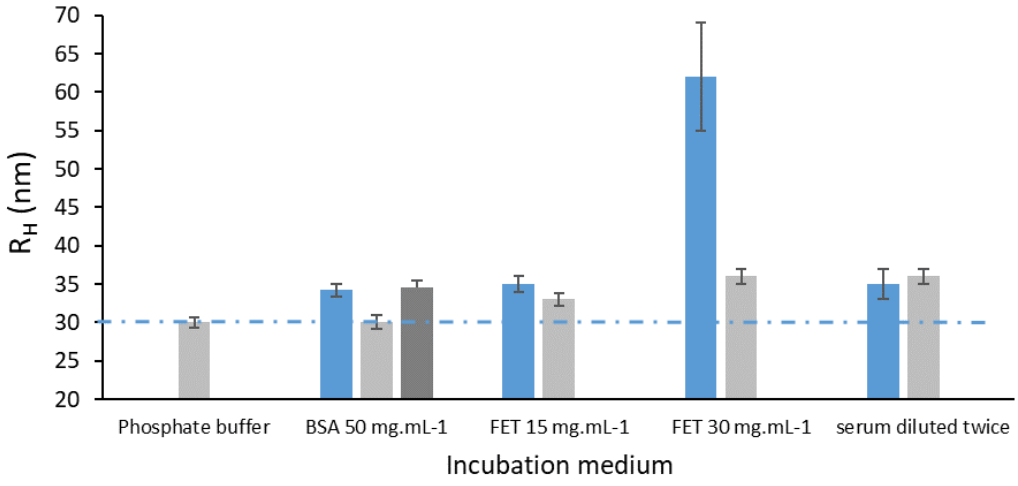

Fig. 5: Mean hydrodynamic radius of Au@SiO_x NPs incubated in various incubation media.
Experimental conditions: Au@SiO_x NPs, diluted at 1$mg.mL^{-1}$ in various media; injection 40 mbar 3 s; HPC capillary 75 µm i.d. x 70 cm total length; analysis medium: phosphate buffer after 2h incubation (in light grey), after 4h incubation (in dark grey), and incubation medium (in blue); mobilization pressure 50 mbar

The comparison of the observed radii indicates whether proteins were adsorbed as either a “hard + soft corona” (blue bars in Figure 5) or a hard corona (grey bars in Figure 5).

As can be seen in Figure 5, analyses performed in the phosphate buffer do not allow observing a hard corona composed of BSA on Au@SiO_x NPs after 2 h incubation. Indeed, the radius obtained after analysis in the phosphate buffer of the sample incubated in a BSA-containing medium ((30.0 ± 0.9) nm) is very close to the one observed for the Au@SiO_x NPs suspended in a protein-free incubation medium (phosphate buffer). However, this reversibility seems to depend on the incubation time (see

Supplementary material, section 5). Increasing the incubation time up to 4 h leads to the recovery of the protein corona thickness observed in the BSA medium (4-5 nm), which may reflect the irreversible character of the protein corona. It can then be assumed that the corona formed by BSA on Au@SiO_x NPs after a 2 h - incubation is reversible and dissociates when the medium is switched to phosphate buffer, pH 7.4, whereas the corona formed after a longer incubation time remains present at the NP surface when switching to a free protein medium. Mc Ritchie [30] reported a desorption at pHs far from the BSA pI. Similarly, although Rezwan et al. [31] detected the formation of a corona on 97 nm-silica NPs in suspension in a BSA solution, and no BSA was found to be adsorbed after elimination of free proteins by centrifugation. A reversible corona was also observed by dilution experiments of carboxyl-coated quantum dots in the presence of human serum albumin [32].On the contrary, Galdino *et al.* described both reversible and irreversible adsorption of BSA onto silica NPs upon incubation in a BSA solution at 60 µM (4.16 $mg.mL^{-1}$). A thin layer of protein corona (~ 4nm) was still observed by energy-filtered transmission electron microscopy (EF-TEM) around the silica NPs after several washing steps [17]. Norde *et al.* also reported an irreversible adsorption of BSA on silica upon dilution after a 20h-incubation [33].

In our case, we assume that the protein layer is nearly totally released upon dilution in phosphate buffer after 2 h incubation and that the corona formed by BSA on Au@SiO_x NPs is reversible and dissociates when the medium is switched to phosphate buffer, pH 7.4. However, increasing the incubation time leads to an increase of the hydrodynamic radius, which may reflect the irreversible character of the protein corona. A possible explanation could be that irreversible adsorption of BSA requires structural changes in the adsorbed BSA, which takes more time to occur, as suggested in several papers [33-35].

By dilution in a phosphate medium, a remaining monolayer of FET was found to be irreversibly adsorbed. For both 15 $mg.mL^{-1}$ and 30 $mg.mL^{-1}$ FET solutions, the corona thickness was found to be around 5 nm, which makes unlikely the hypothesis of an irreversible aggregation of the particles. Indeed, the experiment previously carried out with a capillary filled with 30 $mg.mL^{-1}$ FET showed an

increment in the apparent radius of the NPs around 32 nm, after 80 min incubation in the FET solution. As previously stated, this size, observed by TDA-ICP-MS performed in the 30 $mg.mL^{-1}$ FET incubation medium, corresponds either to the reversible interactions of protein aggregates induced by the NPs or to the reversible formation of small NP clusters. By the dilution of NPs in phosphate buffer, the increment in radius was then reduced to a 5 nm thickness. Upon dilution in phosphate, a hard corona of 5 nm thickness was still tethered around the NPs. To conclude from these experiments, we proved that FET has a higher binding affinity than BSA for the $Au@SiO_x$ NP surface. FET was also noticed to exhibit a higher affinity than BSA for gold NPs [36].

The $Au@SiO_x$ NPs were then incubated in 50% serum for two hours before TDA-ICP-MS analysis. As evidenced by the absence of R_H variations in diluted serum experiments using both conditions (50% serum and phosphate buffer), an irreversible adsorption seemed to occur. This behaviour cannot be explained by BSA adsorption and therefore, this very abundant protein does not seem to dictate the fate of $Au@SiO_x$ NPs in serum. However, the presence of FET in serum cannot explain such a corona. Indeed, as shown in Table 1, neither a hard nor a soft corona was observed for FET concentrations representative of concentrations found in serum (0.8 $mg.mL^{-1}$).

4. Conclusion

In this work, TDA-ICP-MS sizing experiments was shown to provide insight into corona formation of metal-containing NPs from only 25 µL sample volumes. NPs size measurements were achieved in media containing high concentrations of proteins, similar to serum. Variations of hydrodynamic radii of about 15 % can significantly be recorded. The values of protein corona thickness reflect the adsorption of a protein monolayer for both proteins on the $Au@SiO_x$ NPs surface. This method was shown to successfully overcome the limitations of DLS in such concentrated media. However, like DLS, TDA-ICP-MS is not able to distinguish an increase in size due to the formation of a large corona from the one due to aggregation without additional experiments.

By a simple experimental design, the reversible/irreversible character of the protein adsorption can be assessed. Experiments performed in non-equilibrium conditions show that BSA dissociates rapidly after a 2h-incubation , unlike BSA after a longer incubation, FET, and serum constituents for which the monolayer remains unchanged in size. This seems to indicate that BSA cannot be used as a representative model of serum for these Au@SiO_x NPs, as its binding affinity was revealed to be lower than that of some of the serum constituents.

Hence, TDA-ICP-MS can be a valuable tool to measure corona thickness of metallic NPs dispersed in solutions with high concentrations of proteins and can be applied not only to Au@SiO_x NPs but also to other metal-containing particles or elemental-tagged nanoparticles. However, this method is at present limited to NPs under 70 nm (R_H = 35 nm), due to the signal-to-noise ratio of the method, which limits accuracy when size increases. This size limitation allows anyway its use for the vast majority of metal-containing particles designed for nanomedicine's purposes.

Declaration of competing interest

The authors have declared no conflict of interest.

Acknowledgement

This work was supported by the Institute of Chemistry Lyon (Coronano project) and by a French Government Grant managed by the French National Research Agency (ANR-18-CE17-0025-02).

CRediT authorship contribution statement

Arthur Degasperi: Investigation. Lucie Labied: Validation, Software. Carole Farre: Resources, Writing - review & editing. Emmanuel Moreau: Writing - Review & Editing. Carole Chaix: Funding acquisition, Writing - Review & Editing. Matteo Martini: Funding acquisition, Resources, Writing - Original Draft,

Review & Editing. Agnès Hagège: Funding acquisition, Project administration, Conceptualization, Methodology, Writing – Original draft, review & editing, Supervision.

References

[1] H. Huang, W. Feng, Y. Chen, J. Shi, Inorganic nanoparticles in clinical trials and translations, Nanotoday 35 (2020) 100972. https://doi.org/10.1016/j.nantod.2020.100972.

[2] W. Park, H. Shin , B. Choi , W. K. Rhim, K. Na, D. K. Han , Advanced hybrid nanomaterials for biomedical applications, Prog. Mater. Sci. 114 (2020) 100686. https://doi.org/10.1016/j.pmatsci.2020.100686.

[3] G De Crozals, R Bonnet, C Farre, C Chaix, Nanoparticles with multiple properties for biomedical applications: A strategic guide, Nanotoday 11 (2016) 435-463. https://doi.org/10.1016/j.nantod.2016.07.002.

[4] A. Lesniak, F. Fenaroli, M. P. Monopoli, C. Åberg, K. A. Dawson, A. Salvati, Effects of the Presence or Absence of a Protein Corona on Silica Nanoparticle Uptake and Impact on Cells, ACS Nano 6 (2012) 5845–5857. https://doi.org/10.1021/nn300223w.

[5] N. Singh, C. Marets, J. Boudon, N. Millot, L. Saviot, L. Maurizi, In vivo protein corona on nanoparticles: does the control of all material parameters orient the biological behaviour? Nanoscale Adv., 3 (2021) 1209–1229. https://doi.org/10.1039/D0NA00863J

[6] S. Milani, F. Baldelli Bombelli, A.S. Pitek, K.A. Dawson, J. Rädler, Reversible versus Irreversible Binding of Transferrin to Polystyrene Nanoparticles: Soft and Hard Corona, ACS Nano 6 (2012), 2532-2541. https://doi.org/10.1021/nn204951s.

[7] Kari, O. K., Ndika, J., Parkkila P., Louna A., Lajunen T., Puustinen A., Viitala T., Alenius H., Urtti A. In situ analysis of liposome hard and soft protein corona structure and composition in a single label-free workflow, Nanoscale, 12 (2020) 1728-1741. https://doi.org/10.1039/C9NR08186K

[8] Wang Q., Lim M., Liu X., Wang Z., Chen K. L., Influence of Solution Chemistry and Soft Protein Coronas on the Interactions of Silver Nanoparticles with Model Biological Membranes, Environ. Sci. Technol., 50 (2016) 2301–2309. https://doi.org/10.1021/acs.est.5b04694.

[9] T. Cedervall, I. Lynch, S. Lindman, T. Berggård, E. Thulin, H. Nilsson, K. A. Dawson, S. Linse, Understanding the nanoparticle–protein corona using methods to quantify exchange rates and affinities of proteins for nanoparticles, Proc. Natl. Acad. Sci. USA 104 (2007) 2050-2055. https://doi.org/10.1073/pnas.0608582104.

[10] A. Kurtz-Chalot, C. Villiers, J. Pourchez, D. Boudard, M. Martini, P.N. Marche, M. Cottier, V. Forest, Impact of silica nanoparticle surface chemistry on protein corona formation and consequential interactions with biological cells, Mat. Sci. Eng. C 75 (2017) 16-24. https://doi.org/10.1016/j.msec.2017.02.028.

[11] N. Fernández-Iglesias, J.Bettmer, Complementary mass spectrometric techniques for the quantification of the protein corona: a case study on gold nanoparticles and human serum proteins, Nanoscale 7 (2015) 14324-14331. https://doi.org/10.1039/C5NR02625C.

[12] M. Dell'Aglio, Z. Salajkova , A. Mallardi , M.C. Sportelli , J. Kaiser, N. Cioffi , A. De Giacomo, Sensing nanoparticle-protein corona using nanoparticle enhanced Laser Induced Breakdown Spectroscopy signal enhancement, Talanta 235 (2021) 122741. https://doi.org/10.1016/j.talanta.2021.122741.

[13] M. Matczuk, K. Anecka, F. Scaletti,L. Messori, B. K. Keppler, A. R. Timerbaev, M. Jarosz, Speciation of metal-based nanomaterials in human serum characterized by capillary electrophoresis coupled to ICP-MS: a case study of gold nanoparticles, Metallomics, 7 (2015) 1364—1370, https://doi.org/ 101039/c5mt00109a.

[14] M. Matczuk, J. Legat, S. N. Shtykov, M. Jarosz, A. R. Timerbaev, Characterization of the protein corona of gold nanoparticles by an advanced treatment of CE-ICP-MS data, Electrophoresis, 37 (2016) 2257–2259, https://doi.org/10.1002/elps.201600152.

[15] K. Fischer, M. Schmidt, Pitfalls and novel applications of particle sizing by dynamic light scattering. Biomaterials 2016, 98:79–91. https://doi.org/10.1016/j.biomaterials.2016.05.003.

[16] Moya C, Escudero R, Malaspina DC, de la Mata M, Hernández-Saz J, Faraudo J, et al., Insights into Preformed Human Serum Albumin Corona on Iron Oxide Nanoparticles: Structure, Effect of Particle Size, Impact on MRI Efficiency, and Metabolization. ACS Appl. Bio Mater. 2 (2019) 3084-94. https://doi.org/10.1021/acsabm.9b00386.

[17] F.E Galdino, A.S. Picco, L.B. Capeletti, J. Bettini, M.B. Cardoso, Inside the Protein Corona: From Binding Parameters to Unstained Hard and Soft Coronas Visualization Nano Lett. 21 (2021) 8250-8257. https://doi.org/10.1021/acs.nanolett.1c02416.

[18] H. Wang, Y. Lin, K. Nienhaus, G.U. Nienhaus, The protein corona on nanoparticles as viewed from a nanoparticle-sizing perspective, WIREs Nanomed Nanobiotechnol 2017, e1500. https://doi.org/10.1002/wnan.1500.

[19] L. Treuel, S. Brandholt, P. Maffre,S. Wiegele, L. Shang, G. U. Nienhaus, Impact of protein modification on the protein corona on nanoparticles and nanoparticle-cell interactions. ACS Nano 8 (2014) 503–513. https://doi.org/10.1021/nn405019v.

[20] P. Maffre, K. Nienhaus, F. Amin, W. J. Parak, G. U. Nienhaus, Characterization of protein adsorption onto FePt nanoparticles using dual-focus fluorescence correlation spectroscopy, Beilstein J Nanotechnol, 2011, 2, 374–383. https://doi.org/10.3762/bjnano.2.43.

[21] L. Labied, P. Rocchi, T. Doussineau, J. Randon, O. Tillement, F. Lux, A. Hagège, Taylor dispersion analysis coupled to ICP-MS for ultrasmall nano-particle size measurement: from drug product to biological media studies, Anal. Chem., 93 (2021) 1254-1259. https://doi.org/10.1021/acs.analchem.0c03988.

[22] L. Labied, P. Rocchi, T. Doussineau, J. Randon, O. Tillement, H. Cottet, F. Lux, A. Hagège, Biodegradation of metal-based ultra-small nanoparticles: a combined approach using TDA-ICP-MS and CE-ICP-MS, Anal. Chim. Acta, 1185 (2021) 339081. https://doi.org/10.1016/j.aca.2021.339081.

[23] M. Martini, P. Perriat, M. Montagna, R. Pansu, C. Julien, O. Tillement, S. Roux, How gold particles suppress concentration quenching of fluorophores encapsulated in silica beads, J. Phys. Chem. C 113 (2009) 17669–17677. https://doi.org/10.1021/jp9044572.

[24] Chamieh, J.; Leclercq, L.; Martin, M.; Slaoui, S.; Jensen, H.; Østergaard, J.; Cottet, H. Limits in Size of Taylor Dispersion Analysis: Representation of the Different Hydrodynamic Regimes and Application to the Size-Characterization of Cubosomes, Anal Chem 89 (2017) 13487–13493. https://doi.org/10.1021/acs.analchem.7b03806.

[25] E. Pacard, M.A. Brook, A.M. Ragheb, C. Pichot, C.Chaix, Elaboration of silica colloid/polymer hybrid support for oligonucleotide synthesis, Colloids Surf. B 47 (2006) 176-188. https://doi.org/10.1016/j.colsurfb.2005.12.008.

[26] P.-E. Rouet, C. Chomette, L. Adumeau, E. Duguet, S. Ravaine, Colloidal chemistry with patchy silica nanoparticles, Beilstein J. Nanotechnol. 9 (2018) 2989–2998. https://doi.org/10.3762/bjnano.9.278.

[27] Monopoli M. P., Walczyk D., Campbell A., Elia G., Lynch I., Baldelli Bombelli F, Dawson K. A., Physical-Chemical Aspects of Protein Corona: Relevance to in Vitro and in Vivo Biological Impacts of Nanoparticles, J. Am. Chem. Soc 133 (2011) 2525-2534. https://doi.org/10.1021/ja107583h

[28] Orts-Gil, G., Natte, K., Thiermann, R., Girod, M., Rades, S., Kalbe, H., Thunemann, A. F., Maskos, M., Osterle, W., On the role of surface composition and curvature on biointerface formation and colloidal stability of nanoparticles in a protein-rich model system, Colloids Surf. B 108 {2013) 110-119. https://doi.org/10.1016/j.colsurfb.2013.02.027

[29] H. Wang, R. Ma, K. Nienhaus, G.U. Nienhaus, Formation of a Monolayer Protein Corona around Polystyrene Nanoparticles and Implications for Nanoparticle Agglomeration, Small 15 (2019) 1900974. https://doi.org/10.1002/smll.201900974.

[30] Mc Ritchie F., The adsorption of proteins at the solid/liquid interface, J. Colloid Int. Sci. 38 (1972) 434-438. https://doi.org/10.1016/0021-9797(72)90264-0

[31] K. Rezwan, L. P. Meier, L. J. Gauckler, Lysozyme and bovine serum albumin adsorption on uncoated silica and AlOOH-coated silica particles: the influence of positively and negatively charged oxide surface coatings, Biomaterials, 26 (2005) 4351-4357. https://doi.org/10.1016/j.biomaterials.2004.11.017.

[32] H.X. Wang, L.Shang, P.Maffre, S. Hohmann, F. Kirschhoffer, G. Brenner-Weiss, G.U. Nienhaus, The Nature of a Hard Protein Corona Forming on Quantum Dots Exposed to Human Blood Serum, Small 12 (2016) 5836-5844. https://doi.org/10.1002/smll.201602283.

[33] W. Norde, A.C.I; Anusiem, Adsorption, desorption and re-adsorption of proteins on solid surfaces, Colloids Surf. 66 (1992) 73–80. https://doi.org/10.1016/0166-6622(92)80122-I

[34] Giacomelli C.E., Norde W., The Adsorption–Desorption Cycle. Reversibility of the BSA–Silica System J. Colloid Int. Sci. 233 (2001) 234–240. https://doi.org/10.1006/jcis.2000.7219

[35] Kondo A., Oku S., Higashitani K.,Structural Changes in Protein Molecules Adsorbed on Ultrafine Silica Particles, J. Colloid Int. Sci. 143 (1991) 214-221. https://doi.org/10.1016/0021-9797(91)90454-G

[36] H. Moustaoui, J. Saber, I. Djeddi,Q. Liu, D. Movia, A. Prina-Mello, J. Spadavecchia, M. Lamy de la Chapelle, N. Djaker, A protein corona study by scattering correlation spectroscopy: a comparative study between spherical and urchin-shaped gold nanoparticles Nanoscale 11 (2019) 3665–3673. https://doi.org/10.1039/C8NR09891C.

.